NPS67-81-012

# NAVAL POSTGRADUATE SCHOOL

## Monterey, California


MODELING SOLID-FUEL RAMJET COMBUSTION
INCLUDING RADIATION HEAT TRANSFER TO THE FUEL SURFACE

Michael E. Metochianakis
William V. Goodwin
Uri Katz
David W. Netzer

August 1981

Interim Report for 1981

Approved for public release; distribution unlimited

Prepared for:
Naval Weapons Center
China Lake, California

NAVAL POSTGRADUATE SCHOOL

Monterey, California

Rear Admiral J. J. Ekelund
Superintendent

D. A. Schrady
Acting Provost

The work reported herein was supported by the Naval Weapons Center, China Lake, California.



This report was prepared by:

## REPORT DOCUMENTATION PAGE

READ INSTRUCTIONS BEFORE COMPLETING FORM

| | |
|---|---|
| 1. REPORT NUMBER: NPS67-81-012 | 2. GOVT ACCESSION NO. |
| 3. RECIPIENT'S CATALOG NUMBER | |
| 4. TITLE (and Subtitle): Modeling Solid-Fuel Ramjet Combustion Including Radiation Heat Transfer to the Fuel Surface | 5. TYPE OF REPORT & PERIOD COVERED: Interim Report 1981 |
| | 6. PERFORMING ORG. REPORT NUMBER |
| 7. AUTHOR(s): Michael E. Metochianakis, William V. Goodwin, Uri Katz, David W. Netzer | 8. CONTRACT OR GRANT NUMBER(s) |
| 9. PERFORMING ORGANIZATION NAME AND ADDRESS: Naval Postgraduate School, Monterey, California 93940 | 10. PROGRAM ELEMENT, PROJECT, TASK AREA & WORK UNIT NUMBERS: N605308WR30053 |
| 11. CONTROLLING OFFICE NAME AND ADDRESS: Naval Weapons Center, China Lake, California | 12. REPORT DATE: August 1981 |
| | 13. NUMBER OF PAGES: 40 |
| 14. MONITORING AGENCY NAME & ADDRESS (if different from Controlling Office) | 15. SECURITY CLASS. (of this report): UNCLASSIFIED |
| | 15a. DECLASSIFICATION/DOWNGRADING SCHEDULE |

16. DISTRIBUTION STATEMENT (of this Report)

Approved for public release; distribution unlimited

17. DISTRIBUTION STATEMENT (of the abstract entered in Block 20, if different from Report)

18. SUPPLEMENTARY NOTES

19. KEY WORDS (Continue on reverse side if necessary and identify by block number)

Solid Fuel Ramjet

Computer Model

Radiation

20. ABSTRACT (Continue on reverse side if necessary and identify by block number)

Radiation heat transfer from soot in the flame zone to the fuel surface of a solid fuel ramjet was incorporated into an existing two-dimensional computer code. Improved prediction of the fuel regression pattern was obtained. Near-wall temperature measurements indicated that the model predicts too much turbulent mixing near the fuel surface.

TABLE OF CONTENTS

## LIST OF TABLES

## LIST OF FIGURES

## TABLE OF SYMBOLS

| | |
|---|---|
| $A^*$ | Throat area |
| BP | Mass transfer number (or "blowing parameter") |
| $C_D$, $C_1$, $C_2$ | Turbulence model empirical constants (Table I ) |
| $C_p$ | Specific heat at constant pressure |
| f | Fuel |
| g | Mass transfer conductance |
| $g_c$ | Newton constant |
| G | Mass flux |
| gr | Gram |
| h | Step height; enthalpy |
| $\tilde{h}$ | Stagnation enthalpy |
| H | Dimensionless enthalpy |
| i | Stoichiometric coefficient |
| k | Turbulence kinetic energy |
| L | Length of the control volume (cell) |
| m | Mass fraction |
| $\dot{m}$ | Mass flow rate |
| $\dot{m}''$ | Mass flux |
| n | Number density of particulates in the flame zone |
| P | Pressure |
| Pc | Combustion pressure |
| $\dot{q}''$ | Heat flux |

| | |
|---|---|
| $r$ | Radial distance |
| $R$ | Gas constant |
| RR, $\dot{r}$ | Regression rate |
| $S$ | Source term |
| $T$ | Temperature |
| $u$ | Axial velocity |
| $v$ | Radial velocity |
| Vol | Volume |
| $w_{fu}$ | Mass of unburned fuel in the boundary layer |
| $w_{mix}$ | Mass of mixture |
| $x$ | Axial distance |
| $y_p^+$ | Dimensionless distance from the wall |

GREEK SYMBOLS

| | |
|---|---|
| $\alpha$ | Empirical constant (Eq22) |
| $\gamma$ | Ratio of specific heats |
| $\Gamma$ | Effective transport coefficient |
| $\delta$ | Incremental distance from wall (Eq11); thickness of the combustion zone (Eq22) |
| $\Delta H$ | Heat of combustion per Kg of fuel |
| $\Delta w_f$ | Weight loss of fuel |
| $\varepsilon$ | Turbulence dissipation rate; emissivity |
| $\varepsilon_g$ | Emissivity of the flame zone |
| $\lambda$ | Empirical constant (Eq27) |
| $\mu$ | Viscosity |
| $\rho$ | Density |

| | |
|---|---|
| $\sigma$ | Prandtl or Schmidt Number; Stefan-Boltzmann constant $(5.669 \times 10^{-8} \frac{w}{m^2 \, ^oK^4})$ |
| $\tau$ | Shear stress |
| $\Phi$ | Any of the variables: u, v, k, $\varepsilon$, $\tilde{h}$, $\chi = (m_{fu} - \frac{m_{ox}}{i})$; equivalence ratio |
| $\Phi_c$ | Conserved property |
| $\chi$ | $m_{fu} - \frac{m_{ox}}{i}$ |
| $\Psi$ | Stream function |
| $\omega$ | Vorticity |

SUBSCRIPTS

| | |
|---|---|
| burn | Burning |
| bw | "Blowing wall" (fuel surface) |
| c | Combustion |
| con | Convection |
| f | Flame; fuel |
| fu | Fuel |
| fg | Fuel grain |
| in | Inlet |
| lam | Laminar |
| $N_2$ | Nitrogen |
| Ox | Oxygen |
| p | Near wall node, primary, port |
| Pr | Products |
| rad | Radiation |

| | |
|---|---|
| ref | Reference |
| s | Secondary |
| T | Total |
| w | Wall |

# I. INTRODUCTION

During the past decade, there have been many advancements in the development of highly effective tactical weapons for use at intermediate range and with high average flight speed. One of the simplest is the solid fuel ramjet (SFRJ).

The solid fuel ramjet most often consists of a solid fuel grain which provides the walls for the combustion chamber [Ref. 1]. A sudden expansion at the air inlet end of the combustor can be used to provide flame stabilization in the SFRJ (Fig. 1). Combustion can be sustained throughout the fuel grain provided that the step height (h) is sufficiently large. However, the larger is the step height, the larger the losses in inlet stagnation pressure.

Due to the sudden expansion, two distinct flow fields are generated within the fuel grain. In the first one, the recirculation zone, the flow in highly turbulent and normally fuel rich. This hot gas region provides the energy necessary for sustaining the combustion process which must occur further downstream. Downstream of the flow reattachment a turbulent boundary layer develops and the combustion is similar to that in a hybrid rocket, namely diffusion controlled. A diffusion flame emanates from the recirculation zone and remains within the developing turbulent boundary layer between the fuel rich zone near the wall and the oxygen rich central core. Due to that diffusion flame, heat is transferred by convection and radiation to the solid surface which causes vaporization of the fuel. The radiative and convective heat transfer mechanisms are

not independent. The presence of radiation tends to increase the rate of vaporization and this in turn tends to reduce the heat transfer to the wall by convection.

Some of the fuel leaving the grain surface fails to reach the flame by the end of the fuel grain, remaining instead in the boundary layer zone below the flame. This stratified boundary layer exits from the aft end of the fuel grain and may result in decreased combustion efficiency if the fuel is not consumed before entering the exhaust nozzle. In order to increase the combustion efficiency, an aft mixing chamber downstream of the fuel grain (Fig. 1) is often employed. This allows additional chemical reaction of the unburned fuel to take place. To promote mixing in that region and to increase the allowable fuel loading, a portion of the inlet air is sometimes bypassed to the region aft of the fuel grain.

There have been continuing research efforts concerned with the combustion behavior of the SFRJ at the Naval Postgraduate School, the Naval Weapons Center, and the United Technologies Corporation/CSD. At NPS, both mathematical modeling and experimental efforts [Ref. 2, 3, 4, 5, 6] have been conducted to determine the effects of design and operational variables on the obtainable performance.

The computer model simulation of the SFRJ combustion process has evolved from an original stream-function vorticity formulation [Ref. 1] to a primitive-variable (pressure, velocity) model which includes the aft mixing chamber [Ref. 7]. These models have not included radiative heat transfer to the fuel surface. This has limited the utility of the model since many all-hydrocarbon fuels produce significant amounts of radiative heat transfer through the generation of carbon particulates in

the flame zone. The purpose of the present effort was to incorporate into the primitive variable computer model radiative heat transfer from carbon particles within the flame zone to the fuel surface.

## II. DESCRIPTION OF COMPUTER MODEL

### A. INTRODUCTION

At the Naval Postgraduate School there have been two basic computer codes used to model the flow within solid fuel ramjets. The first one was based on vorticity ($\omega$) and stream function ($\psi$) [Ref. 1]. It predicted reasonably accurate velocity and temperature distributions but did not predict pressure distributions accurately and was not easily extended to complex geometries or to three dimensional flows. The second computer model is based on the primitive variables, velocity (u,v) and pressure (p) [Ref. 7]. It has also been used to predict the flowfield within the fuel grain. However the u-v-p model also permitted the prediction of the flowfield within the aft mixing region. The latter model can be used to predict the effects of fuel properties on the SFRJ performance and to evaluate the effects of different geometries and operating conditions. However, only convective heat transfer to the fuel surface has been considered and, therefore, the predicted fuel regression profiles have not been correct for fuel systems (such as HTPB) that generate large amounts of radiative heat transfer to the fuel surface.

In the present work, the primitive variable computer program was modified to include the effect of radiation to the fuel surface from carbon particles within the flame zone. Gas phase radiation was neglected.

### B. OVERVIEW OF PRIMITIVE VARIABLE COMPUTER PROGRAM

#### 1. Assumptions

The CHAMPION 2/E/FIX computer program developed by Pun and Spalding [Ref. 8] was used as the basis for the primitive variable

model. The flow was assumed to be steady, subsonic, recirculating, axisymmetric and to have constant specific heat. To calculate the effective viscosity, a modified Jones-Launder [Refs. 7 - 10] two-parameter turbulence model was used. The combustion was considered to be mixing limited (infinitely fast kinetics) with a simple one-step chemical reaction of the form:

$$1 \text{ kg fuel} + i \text{ kg Oxidizer} \longrightarrow (1 + i) \text{ kg Products}$$

Four species were considered: oxygen, nitrogen, fuel and products. Because of the infinitely fast kinetics assumed, no oxygen could exist at the fuel surface and that surface was considered to be isothermal. The turbulent Lewis number was also taken to be unity.

## 2. Governing Equations and Boundary Conditions

With the above assumptions, the governing equations for axisymmetrical flows can be cast in the following format:

$$\underbrace{\frac{\partial}{\partial x}(\rho u \Phi) + \frac{1}{r}\frac{\partial}{\partial r}(\rho r v \Phi)}_{\text{Convection Terms}} - \underbrace{\frac{\partial}{\partial x}\left(\Gamma_\Phi \frac{\partial \Phi}{\partial x}\right) - \frac{1}{r}\frac{\partial}{\partial r}\left(r\Gamma_\Phi \frac{\partial \Phi}{\partial r}\right)}_{\text{Diffusion Terms}} + \underbrace{S_\Phi}_{\text{Source Terms}} = 0 \qquad (1)$$

where $\Phi$ stands for the variables u, v, k, $\varepsilon$, $\tilde{h}$, $\chi = \left(m_{fu} - \frac{m_{ox}}{i}\right)$ and $m_{N_2}$ ($\Phi = 1$ for the continuity equation). $S_\Phi$ is the "source term" and $\Gamma_\Phi$ is the effective exchange coefficient for turbulent flow (Table I).

Since the quantities $\tilde{h}$ (stagnation enthalpy), $m_{N_2}$ and $\chi = m_{fu} - \frac{m_{ox}}{i}$ have identical governing differential equations and, in appropriate dimensionless form, identical boundary conditions, only one of the equations had to be solved.

| $\Phi$ | $\Gamma_\Phi$ | $S_\Phi$ |
|---|---|---|
| u | $\mu_{eff}$ | $\frac{\partial p}{\partial x} + \frac{2}{3}\frac{\partial}{\partial x}\left\{\frac{\mu}{r}\left[\frac{\partial}{\partial x}(ru) + \frac{\partial}{\partial r}(rv)\right]\right\} - \frac{\partial}{\partial x}\left(\mu\frac{\partial u}{\partial x}\right) - \frac{1}{r}\frac{\partial}{\partial r}\left(\mu r\frac{\partial v}{\partial x}\right)$ |
| v | $\mu_{eff}$ | $\frac{\partial p}{\partial x} + 2\frac{\mu v}{r^2} + \frac{2}{3}\frac{\partial}{\partial r}\left\{\frac{\mu}{r}\left[\frac{\partial}{\partial x}(ru) + \frac{\partial}{\partial r}(rv)\right]\right\} - \frac{\partial}{\partial x}\left(\mu\frac{\partial u}{\partial r}\right) - \frac{1}{r}\frac{\partial}{\partial r}\left(\mu r\frac{\partial v}{\partial r}\right)$ |
| $\varepsilon$ | $\frac{\mu_{eff}}{\sigma_\varepsilon}$ | $-\frac{C_1\varepsilon}{k}\left\{\mu_t\left[2\left[\left(\frac{\partial u}{\partial x}\right)^2 + \left(\frac{\partial v}{\partial r}\right)^2 + \left(\frac{v}{r}\right)^2\right] + \left(\frac{\partial u}{\partial r} + \frac{\partial v}{\partial x}\right)^2\right]\right\} + \frac{C_2\rho\varepsilon^2}{k}$ |
| k | $\frac{\mu_{eff}}{\sigma_k}$ | $\rho\varepsilon - \mu_t\left\{2\left[\left(\frac{\partial u}{\partial x}\right)^2 + \left(\frac{\partial v}{\partial r}\right)^2 + \left(\frac{v}{r}\right)^2\right] + \left(\frac{\partial u}{\partial r} + \frac{\partial v}{\partial x}\right)^2\right\}$ |
| $\tilde{h}$ | $\frac{\mu_{eff}}{\sigma_h}$ | 0 |
| $m_{fu} - \frac{m_{ox}}{i}$ | $\frac{\mu eff}{\sigma_j}$ | 0 |
| $m_{N_2}$ | $\frac{\mu_{eff}}{\sigma_j}$ | 0 |

$C_1 = 1.43$, $C_2 = 1.92$, $\sigma_j = \sigma_k = \sigma_h = 1$, $\sigma_\varepsilon = 1.3$

TABLE I. Governing Equation Parameters

The dimensionless enthalpy was selected to be:

$$H = \frac{\tilde{h}_{in} - \tilde{h}}{\tilde{h}_{in} - \tilde{h}_{fg}} \tag{2}$$

where $\tilde{h}_{fg}$ is the enthalpy deep in the fuel grain and $\tilde{h}_{in}$ the enthalpy of the air at the inlet dump plane. The corresponding dimensionless forms for the other properties were:

$$\bar{m}_{N_2} = \frac{m_{N_{2_{in}}} - m_{N_2}}{m_{N_{2_{in}}} - m_{N_{2_{fg}}}} \tag{3}$$

and:

$$\bar{\chi} = \frac{\chi - \chi_{in}}{\chi_{fg} - \chi_{in}} \tag{4}$$

The solution of the governing differential equation for $\tilde{h}$ permitted calculation of H which was numerically equal to $\bar{m}_{N_2}$ and $\bar{\chi}$. The values of $m_{N_2}$ and $\chi$ were then obtained using equations (3) and (4).

From

$$\tilde{h} \equiv h + \frac{u^2 + v^2}{2} + k \tag{5}$$

h was determined. This, in turn, permitted the calculation of temperature (T) from the relation:

$$h \equiv \frac{m_{ox}\Delta H}{i} + C_p (T - T_{ref}) \tag{6}$$

Equation (6) is a simplified method for accounting for the heats of formation and results when all of the heat of combustion ($J/kg_{fuel}$) is "attached" to the oxidant [Ref. 11].

The density was calculated from the perfect gas law:

$$\rho = \frac{P}{RT} \tag{7}$$

in which R was calculated using the average molecular weight ($R = \frac{\bar{R}}{\bar{M}}$)

The mass fractions of fuel ($m_{fu}$), oxygen ($m_{ox}$) and products ($m_{pr}$) were calculated from the relations:

$$\begin{aligned} \chi \geq 0;\ m_{fu} &= \chi,\ m_{ox} = 0 \\ \chi < 0;\ m_{fu} &= 0,\ m_{ox} = -\chi i \end{aligned} \tag{8}$$

and:

$$m_{pr} = 1 - m_{ox} - m_{fu} - m_{N_2} \tag{9}$$

In order to calculate the wall shear stress ($\tau_w$), a two part boundary layer was used. The division between the laminar sublayer and the turbulent layer was assumed to be at $Y_p^+ = 11.5$ [Ref. 8].

Then, if $Y_p^+ \geq 11.5$, the wall shear stress ($\tau_w$) was calculated in terms of the near-wall kinetic energy of turbulence using the relation:

$$\tau_w = C_D^{1/2} \rho k_p ; \tag{10}$$

whereas, if $y_p^+ < 11.5$, $\tau_w$ was found assuming a linear velocity profile from the formula:

$$\tau_w = \mu_{lam} \frac{u_p}{\delta} \tag{11}$$

$\tau_w$ provided the boundary conditions for the u and v equations.

Since $\tilde{h}$, $m_{N_2}$ and $\chi = m_{fu} - \frac{m_{ox}}{i}$ are considered to be "conserved properties" [Ref. 11], the boundary condition for all of them can be written in the form:

$$\dot{m}''_{bw} = \frac{(\Gamma_\Phi \frac{\partial \Phi_c}{\partial r})_{bw}}{\Phi_{c_{bw}} - \Phi_{c_{fg}}} \tag{12}$$

where $\Phi_c$ stands for $\tilde{h}$, $m_{N_2}$ or $\chi$.

The mass transfer conductance (g) is generally defined to be:

$$g = \frac{(\Gamma_\Phi \frac{\partial \Phi_c}{\partial r})_{bw}}{\Phi_{c_\infty} - \Phi_{c_{bw}}} \tag{13}$$

g can also be equated to $\frac{\tau_w}{u_p}$ [Ref. 7]. Equations (12) and (13) result in:

$$\dot{m}''_{bw} = g \frac{\Phi_{c_p} - \Phi_{c_{bw}}}{\Phi_{c_{bw}} - \Phi_{c_{fg}}} \tag{14}$$

where the near-wall grid value ($\Phi_{c_p}$) has been used in place of the "free stream" value ($\Phi_{c_\infty}$).

The mass transfer parameter is given by:

$$BP \equiv \frac{\Phi_{c_p} - \Phi_{c_{bw}}}{\Phi_{c_{bw}} - \Phi_{c_{fg}}} = \frac{\tilde{h}_p - \tilde{h}_{bw}}{\tilde{h}_{bw} - \tilde{h}_{fg}} \tag{15}$$

Therefore (14) and (15) result in:

$$\dot{m}''_{bw} \equiv gBP \tag{16}$$

Solution of the stagnation enthalpy allowed calculation of the blowing parameter using (15).

The wall shear stress calculated for no wall mass addition ((10) or (11)) was then modified for blowing using the Couette flow approximation [Ref. 11]:

$$\tau_{bw} = \tau_w \frac{\ln (1 + BP)}{BP} \tag{17}$$

g can then be calculated from $\tau_{bw}/u_p$ and $\dot{m}''_{bw}$ calculated using (16). The convective flux ($\dot{q}''_{con}$) on all boundaries was calculated using a modified Reynolds analogy:

$$\dot{q}''_{con} = (\tilde{h}_p - \tilde{h}_w) \frac{\tau_{bw}}{u_p} \tag{18}$$

where the values of $\tilde{h}$ and u at the near wall node point (p) have been used in place of the values at the edge of the boundary layer.

The fuel regression rate (RR) and the blowing velocity ($V_{bw}$) were calculated from:

$$RR = \frac{\dot{m}''_{bw}}{\rho_{fg}} \tag{19}$$

$$v_{bw} = - \frac{\dot{m}''_{bw}}{\rho_{bw}} \tag{20}$$

3. Solution Procedure

Using equation (1) in finite difference form, the variables: u, v, k, $\varepsilon$ and $\tilde{h}$ were found. The line by line iterative procedure employed upwind differencing and under relaxation to promote convergence [Ref. 8]. Imposing mass and momentum conservation on each radial grid line and in

each nodal control volume, the pressure (relative to a selectable position and magnitude within the grid) was obtained. The effective viscosity, density and temperature were also obtained as described above. More details of the solution procedure can be found in Reference 8.

## C. MODIFICATION TO INCLUDE RADIATION TO THE FUEL SURFACE

### 1. Introduction

The regression rate of the fuel is proportional to the total heat transfer to the surface. This heat transfer consists of two interdependent parts, convection and radiation. The presence of radiation tends to increase the rate of fuel decomposition/vaporization and this in turn tends to reduce the heat transfer to the wall by convection.

The convective heat transfer depends on the flow conditions within the port of the fuel grain; primarily upon the air temperature and the air mass flow per unit area.

The radiant energy to the fuel surface can be approximated by:

$$\dot{q}''_{rad} = \sigma\varepsilon_w \left[ \varepsilon_g T_f^4 - T_w^4 \right] \qquad (21)$$

where: $\varepsilon_w$ = the emissivity and absorptivity of the wall

$\sigma$ = the Stefan-Boltzmann constant (= $5.669 \times 10^{-8} \frac{W}{m^2 \cdot K^4}$)

$\varepsilon_g$ = the emissivity of the flame zone

$T_w$ = the wall temperature

$T_f$ = the flame temperature

This simplified approach was taken in keeping with the approaches taken for the combustion process and the wall mass addition.

Radiative heat transfer is a function of the pressure (p) in the combustor, the thickness ($\delta$) of the combustion (flame) zone, the amount of soot, and is strongly dependent on the flame temperature $T_f$.

2. Assumptions

The emissivity of the flame zone can be written [Ref. 12]:

$$\varepsilon_g = 1 - e^{-\alpha n \delta} \tag{22}$$

where $\alpha$ is an empirical constant, $\delta$ is the flame zone thickness and n is the number density of particulates in the flame zone (Fig. 2). In this application, only the dominant effect of radiation from the carbon particles within the flame zone was considered. It was assumed that the gases between the flame and the wall were transparent and that gas phase radiation was negligible.

The number density n of particulates in the flame zone was assumed to be proportional to the number density within the boundary layer and this in turn proportional to the mass density of unburned fuel in the boundary layer. The latter is an assumption that a fixed percentage of the unburned fuel is solids. Thus:

$$n_{flame} \sim n_{\substack{boundary \\ layer}} \sim \frac{\text{Mass of unburned fuel}}{\text{Vol}} \equiv \frac{w_{fu}}{\text{Vol}} \tag{23}$$

But:

$$w_{fu} = w_{mix} \cdot m_{fu} \tag{24}$$

where $w_{mix}$ is the mass of the mixture and $m_{fu}$ is the mass fraction of fuel. Also:

$$w_{mix} = \rho(\text{Vol}) \tag{25}$$

where $\rho$ is the gas density.

Substituting (24) and (25) into (23) yields:

$$n \sim \rho m_{fu} \tag{26}$$

Equation (26) indicates for the simplifications employed in this application that the number density of particulates (n) depends directly on the pressure ($\rho = \frac{P}{RT}$).

The flame zone thickness $\delta$ has been found to be proportional to the square root of the port diameter, but for a given geometry is almost constant [Ref. 12]. Therefore, the effect of $\delta$ can be incorporated into the empirical constant $\alpha$. When these approximations are incorporated into (22) the following expression is obtained:

$$\varepsilon_g \sim 1 - e^{-\frac{\rho m_{fu}}{\lambda}}$$

or

$$\varepsilon_g \equiv 1 - e^{-\frac{w_{fu/Vol}}{\lambda}} \tag{27}$$

where $\lambda$ an empirical constant.

To estimate the mass of unburned fuel in the boundary layer at a particular axial location, a summation was made over control volumes of the finite difference grid from the fuel surface to the axis of symmetry. Thus:

$$w_{fu} = \sum_{cells} w_{fucell} = \sum_{cells} w_{mix} m_{fu} = \sum_{cells} \rho A L m_{fu} \tag{28}$$

Equation (28) was divided by the summation of all control volumes that had finite amounts of fuel present and then substituted into (27) to estimate $\varepsilon_g$.

The mass transfer number BP must also be modified to account for thermal radiation. The modified form of the definition of BP for systems involving radiation heat transfer [Ref. 11] is:

$$BP = \frac{\tilde{h}_p - \tilde{h}_{bw}}{\tilde{h}_{bw} - \tilde{h}_{fg} - \left(\frac{\dot{q}''_{rad}}{\dot{m}''}\right)} \tag{29}$$

In this investigation $T_{wall}$ was taken to be $T_{ref}$ and, therefore, (from (5) and (6)): $\tilde{h}_{bw} = 0$.

Thus:

$$BP = \frac{\tilde{h}_p}{-\tilde{h}_{fg} - \left(\frac{\dot{q}''_{rad}}{\dot{m}''}\right)} \tag{30}$$

where $\dot{q}''_{rad}$ is the radiative heat flux (21) and $\dot{m}''$ the wall mass flux.

3. Solution Procedure

The same solution procedure discussed above for the simple convection model was followed in determining the five variables (u, v, k, $\varepsilon$, $\tilde{h}$). The radiative heat flux was calculated from (21) for fixed values of $\varepsilon_w$, $T_f$ and $T_w$. A corrected blowing parameter was then found from (30), resulting in a modified mass transfer rate (eq (16)). The modified regression rate (RR) and blowing velocity ($v_{bw}$) were obtained from equations (19) and (20).

In order to provide numerical stability the effects of radiation could be omitted for a specified number of initial sweeps through the grid field. This allowed the convective heat transfer solution to converge before introducing the radiative effects.

## III. EXPERIMENTAL MEASUREMENT OF RADIAL TEMPERATURE PROFILES

Two experiments were performed in order to obtain two different radial temperature profiles near the aft end of the fuel grain for two different air flow rates. The intent was to obtain experimental profiles that could be compared with computer generated profiles that are in part dependent upon air flow rate as a data input. The comparison could then be used to assist in the validation of the computer model.

Two Plexiglas fuel grains were identically prepared with eight chromel-alumel thermocouples imbedded 0.0254 m from the aft end of the grain. Four of the eight thermocouples used 36 gage wire while the remaining four were 30 gage (Figure 3).

The four thermocouples of each size were imbedded to distances of 0.51, 2.54, 4.57, and 6.35 mm from the inside grain wall. The thermocouples were also spaced 45 degrees apart from each other.

One test was conducted with 50% bypass air and one without bypass air. The total nominal air flow rate was 0.0907 kg/s. The voltage signals obtained from the thermocouples were input directly into a Visicorder. Temperatures were obtained from the data by comparison of the recorded signals with previously obtained calibration curves (Figure 4). The calibration curves (for both gages of thermocouples) were necessary since the experiments were conducted without the use of an ice bath or other type of reference junction. The calibration consisted of using an oxy-acetylene torch as a heat source for the thermocouples that were simultaneously being referenced to an electronic ice point. By measuring the temperature induced voltages on a digital voltmeter the deflections on the Visicorder

traces could be related to the temperature induced voltages. The data extraction method consisted of measuring the deflection distance from the Visicorder trace, entering the calibration curve with the distance and obtaining a corresponding voltage which was then used with tables that relate the induced thermocouple voltage to the actual temperature being sensed by the thermocouple (uncorrected for radiation heating).

# IV. DISCUSSION OF RESULTS

## A. INTRODUCTION

In the modifications made to the primitive variable computer program only the dominant effect of radiation from the carbon particles within the flame zone was considered. The radiative heat transfer to the fuel surface was then approximated by equation (21) where the emissivity of the flame zone ($\varepsilon_g$) was taken from the relation (27). The effects of the amount of unburned carbon and the combustor pressure were incorporated into this expression. For the Plexiglas-$O_2$ system (which has only small radiation effects) a typical value for $\varepsilon_g$ is 0.02 and the radiative heat flux to the fuel grain is approximately 15% of the convective flux [Ref. 13]. Using these values the empirical constant ($\lambda$) in equation (27) was found to be approximately 3. For fuel systems that generate larger amounts of radiative heat transfer (for example HTPB) the empirical constant $\lambda$ should be lower than 3.

It was also assumed that the radiation ($\dot{q}''_{rad}$) is absorbed and emitted at least an infinitesimal distance inside the solid surface and that the gases between the flame and the wall were transparent. The region between the flame and the wall was taken to be totally unaffected by the radiation [Ref. 11].

Once numerically stable computer model solutions were obtained, the effects of pressure, inlet velocity and increased $\dot{q}''_{rad}$ (by reducing the empirical constant $\lambda$ for systems that produce large amounts of radiation) were examined.

It has been found experimentally that increased combustor pressure increases the average regression rate. However, for PMM the effect of pressure alone is not large [Ref. 2]. Much of the reported effects of $P_c$ in Ref. 2 appear to have resulted from variations in G or inlet geometry. Small variation in $\dot{r}$ with $P_c$ at fixed G cannot be explained in terms of the convection heat transfer because it normally depends only on mass flux ($G = \frac{\dot{m}}{A_p}$):

$$\dot{q}''_{con} \simeq G^{0.8} = \left(\frac{\dot{m}}{A_p}\right)^{0.8} = \left(\frac{\frac{P}{RT} A_p u}{A_p}\right)^{0.8} = \left(\frac{pu}{RT}\right)^{0.8} \qquad (32)$$

For fixed values of $\dot{m}$ and $A_p$ (i.e., G), $\dot{q}''_{con}$ is independent of pressure since the velocity varies inversely with pressure. Pressure changes that result from decreasing the nozzle throat size necessarily increase $\dot{q}''_{rad}$. Therefore, $\dot{q}''_{rad}$ is thought to be the cause for the observed increased average regression rate with combustor pressure. In some combustion systems finite rate kinetics can also result in significant effects of pressure.

Fuels that generate large amounts of carbon (like HTPB) also result in a different regression rate pattern compared with the pattern obtained using PMM. The main difference is that in the HTPB type systems the regression rates increase with axial distance at the aft end of the grain. One possible cause of such an effect is that as the reacting flow gets hotter and accelerates, convective heat transfer is increased. However, the computer calculations indicated that this was not a dominant effect. Therefore, $\dot{q}''_{rad}$ was again considered to be the reason for this behavior.

The experimentally obtained regression rate pattern for PMM [Ref. 7] is higher than that predicted using the primitive variable computer model with only convective heat transfer, especially at the back of the fuel grain. The flow reattachment point has also been found to occur slightly further downstream than predicted.

B. EFFECT OF RADIATION ON REGRESSION RATE

Figure 5 shows the regression profiles obtained for the two cases: with and without radiation heat transfer to the fuel surface. The flow reattachment point was not affected by incorporation of radiation into the model. Radiation increased the regression rates downstream of reattachment, resulting in a regression profile in better agreement with experiment.

C. EFFECT OF PRESSURE

Figure 6 shows the effects of combustion pressure on the fuel regression rate with radiation. In the first case (nominal $P_c$) the pressure was taken to be $4.826 \times 10^5 \frac{N}{m^2}$ whereas in the other case the chamber pressure was $9.652 \times 10^5 \frac{N}{m^2}$. It can be seen that increased chamber pressure increased the regression rate in general agreement with experimental observations. The reattachment point also moved slightly to the right in this case. Specific experimental data were not available for comparison.

As discussed above, the regression rate of Plexiglas has been reported to vary significantly with chamber pressure [Ref. 2]. Closer examination of that data reveals that for fixed geometry and mass flux

the pressure effect is quite weak. For the two cases considered, the model predicted regression rate to vary as $P_c^{0.06}$. Therefore, the predicted dependence of regression rate on the pressure was very weak and in reasonable agreement with experiment.

D. EFFECT OF INLET AIR MASS FLUX (VELOCITY)

The effect of increasing air mass flux on the regression rate is shown in Figure 7. The regression profile remained the same and, as expected, increased with increasing inlet velocity, $V_{in}$ ($G \sim V_{in}$). It has been found experimentally that the regression rate of Plexiglas varies with the air mass flux (G) as:

$$\dot{r} = C\, G^{y} \tag{33}$$

For the three cases considered here ($V_{in}$ = 158, 197 and 236 $\frac{m}{sec}$) the constant y was predicted to be between 0.23 and 0.28 while Mady et al [Ref. 4] experimentally found it to be approximately 0.38. Therefore, the model appears to correctly predict the nature of the change in convective heat flux to the fuel surface with air flow rate.

E. EFFECT OF INCREASING RADIATION

In fuel systems that produce larger amounts of carbon particulates than the Plexiglas, the empirical constant $\lambda$ must be reduced to less than 3. For the three test cases of this study (Figure 8) the values of $\lambda$ considered were: 3.00, 2.18 and 1.63. Lower values of $\lambda$ resulted in higher regression rates near the aft end of the fuel grain. This results from the increasing amounts of unburned fuel below the flame with increasing axial distance.

## F. DISTRIBUTION OF RADIATION ALONG THE FUEL GRAIN

Figure 9 shows the predicted fraction of the radiative and convective heat fluxes to the fuel surface along the grain for PMM. From the relations (30), (17) and (18) it can be seen that the energy of radiation tends to increase the mass transfer number BP, which decreases the wall shear stress $\tau_{bw}$. This in turn decreases the rate of convective heat transfer to the wall. Thus, increasing radiation produces a decrease in the convection heat trnasfer to the wall as is depicted in Figure 9. The amount of radiation in the model depends strongly upon the empirical constant $\lambda$. This value is selected to match experimental data for one fuel and one set of test conditions. More data are required to determine whether or not one value of $\lambda$ can be used for varying test conditions with one fuel.

## G. COMPARISON OF PREDICTED AND MEASURED TEMPERATURE PROFILES

### 1. Nonbypass Conditions

Figure 10 is a graph of temperature vs. time for seven of the eight thermocouples used in the experiment without bypass air (one small thermocouple showed no response). The similarities in the response times of each of the thermocouples around the circumference indicated that a rather uniform, axisymmetric flame boundary existed at this particular location within the fuel grain.

The actual average regression rate for this experiment was determined to be 0.160 mm/sec, based on the measured weight loss and previous experiments using the same configuration. Using this regression rate and the information from Figure 10, a temperature vs. distance profile was produced as shown in Figure 11. This graph shows the similarities in

each of the profiles for the four heavy gage thermocouples. The graph represents the temperature profiles as they occurred in the fuel grain if the ordinate of the graph is located as shown. This would seemingly contradict, however, the knowledge that the surface temperature of burning PMM is approximately 600 degrees Kelvin. In order to take this into account the profiles need to be shifted either to the left or to the right within a range of 0.76 mm depending upon the thermocouple. Several experimental conditions affected the profiles. The leveling off of the temperature occurred because the thermocouples bent over when they lost strength as they approached the flame. Each thermocouple also generated near-wall mixing and increased the local fuel regression rate. This, in turn, could reduce the local temperature because of the more fuel rich condition that was generated.

2. Bypass Air

This test was made so that a lower air flow velocity in the fuel port could be achieved while still maintaining a choked exhaust nozzle. However, bypass air may affect the temperature profile within the fuel port. To minimize this effect the motor air inlets were operated in a choked condition.

Figure 12 shows the temperature vs. time profiles for six of the eight thermocouples in this experiment. Two of the thermocouples were never exposed to the flame due to the lower regression rate of the bypass configuration. Again there were similarities between all of the profiles.

For this experiment the average regression rate was determined to be 0.109 mm/sec based on the measured weight loss and previous experiments using the same configuration. Figure 13 is a plot of temperature vs.

distance based on this regression rate. This graph shows good agreement between the profiles obtained with the heavy gage thermocouples. In order to bring these profiles to a position that would agree with a 600 degree Kelvin surface temperature, a shift to the left of from 0.57 to 0.70 mm in the profile would be required.

3. Comparison with Computer Model Temperature Profiles

Using the primary air mass flow rate, the chamber pressure and the temperature of the inlet air as inputs to the computer program, temperature vs. distance profiles were predicted as shown in Figures 11 and 13 by the dashed lines. The solid lines represent experimental profiles.

The dashed line in Figure 13 is based on a primary air mass flow rate of 0.0445 kg/sec. For the range of temperatures between 600 and 1000$^{o}$K the profiles were similar. However, above 1000$^{o}$K there was a marked difference between the profiles. This difference was probably due to the fact that the thermocouples had by this time bent over and/or burned out, making them incapable of measuring the higher temperatures encountered. Maximum expected temperatures are approximately 2500$^{o}$K.

The dashed line in Figure 11 was based on an air mass flow rate of 0.088 kg/sec. There was even less agreement between profiles than obtained with bypass air (lower air mass flow rate). Again, this could be attributed to the fact that the thermocouples had ceased to function at a low temperature (approximately 1500$^{o}$K).

Comparison between the theoretical and experimental profiles indicates that the computer model predicts a steeper gradient for both the high and low air flow rates than those that actually occurred in the experiment.

The computer model also predicts a steeper gradient for the higher flow rate, but the experimental results indicate nearly identical gradients for both flow rates.

If the experimental profiles near the fuel surface are even reasonably accurate, it indicates that the computer model predicts more near wall mixing (higher turbulence) than actually occurs.

## V. CONCLUSIONS

Addition of radiative heat transfer to the primitive variable computer model resulted in improved agreement with experimentally obtained fuel regression rate profiles. The effects of varying chamber pressure and air mass flux appear to be qualitatively correct but additional data are required to further validate the model.

Comparison with limited experimental data for radial temperature profiles indicates that the model predicts too high near wall turbulence.

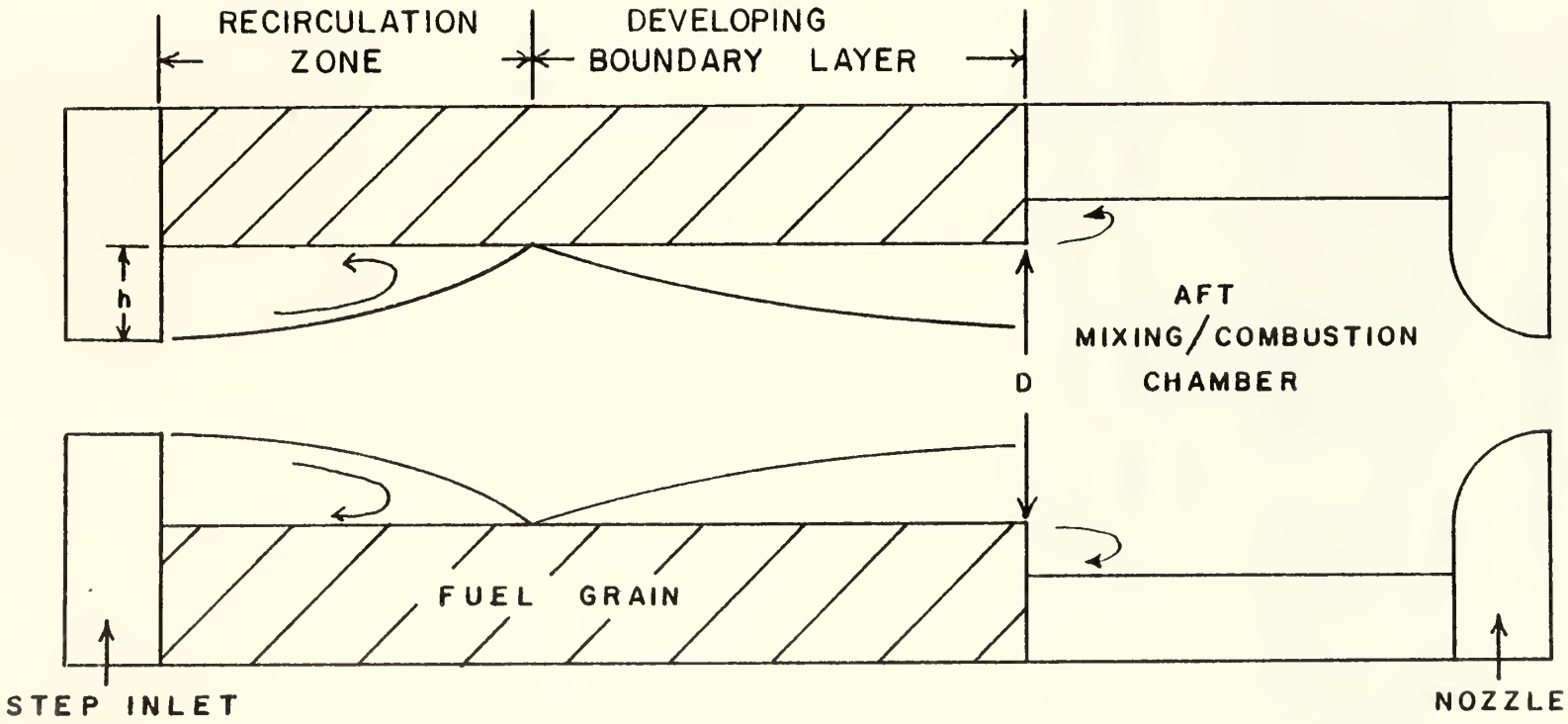


Fig. 1. Schematic of Solid Fuel Ramjet Combustion Regions

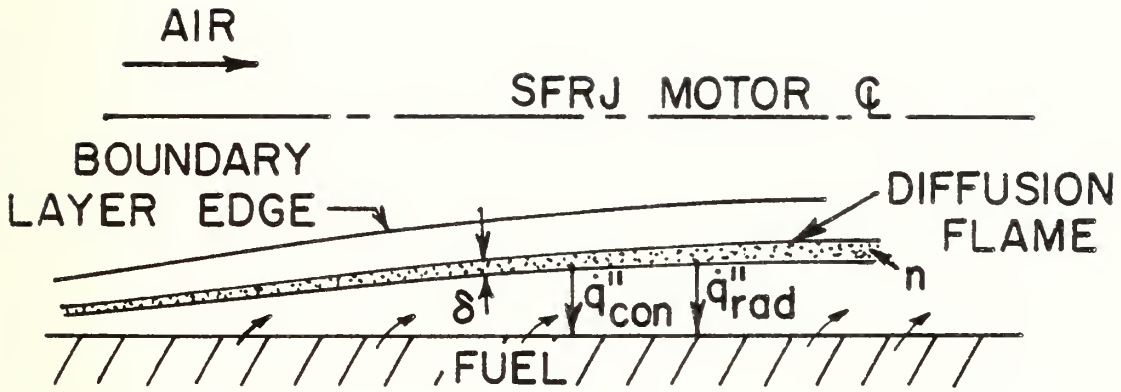


Fig. 2. Schematic of SFRJ Boundary Layer Combustion Process

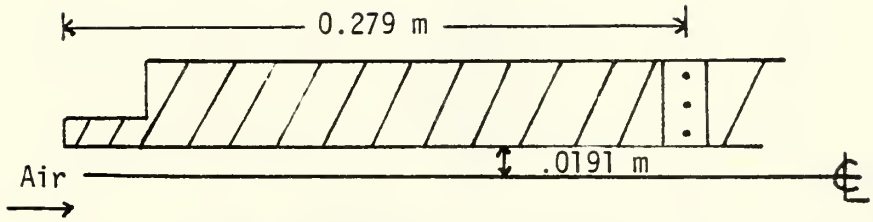


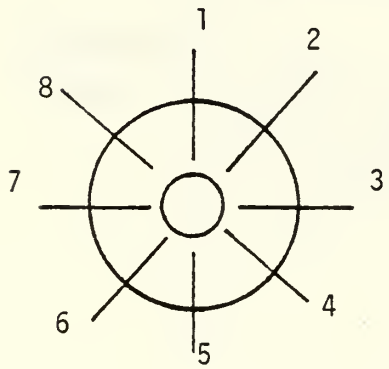


| Thermocouple No. | Gage | Distance from Inside Wall (mm) |
|---|---|---|
| 1 | 30 | 0.51 |
| 2 | 30 | 2.54 |
| 3 | 30 | 4.57 |
| 4 | 30 | 6.35 |
| 5 | 36 | 0.51 |
| 6 | 36 | 2.54 |
| 7 | 36 | 4.57 |
| 8 | 36 | 6.35 |

Figure 3. Schematic of Fuel Grain with Imbedded Thermocouples.

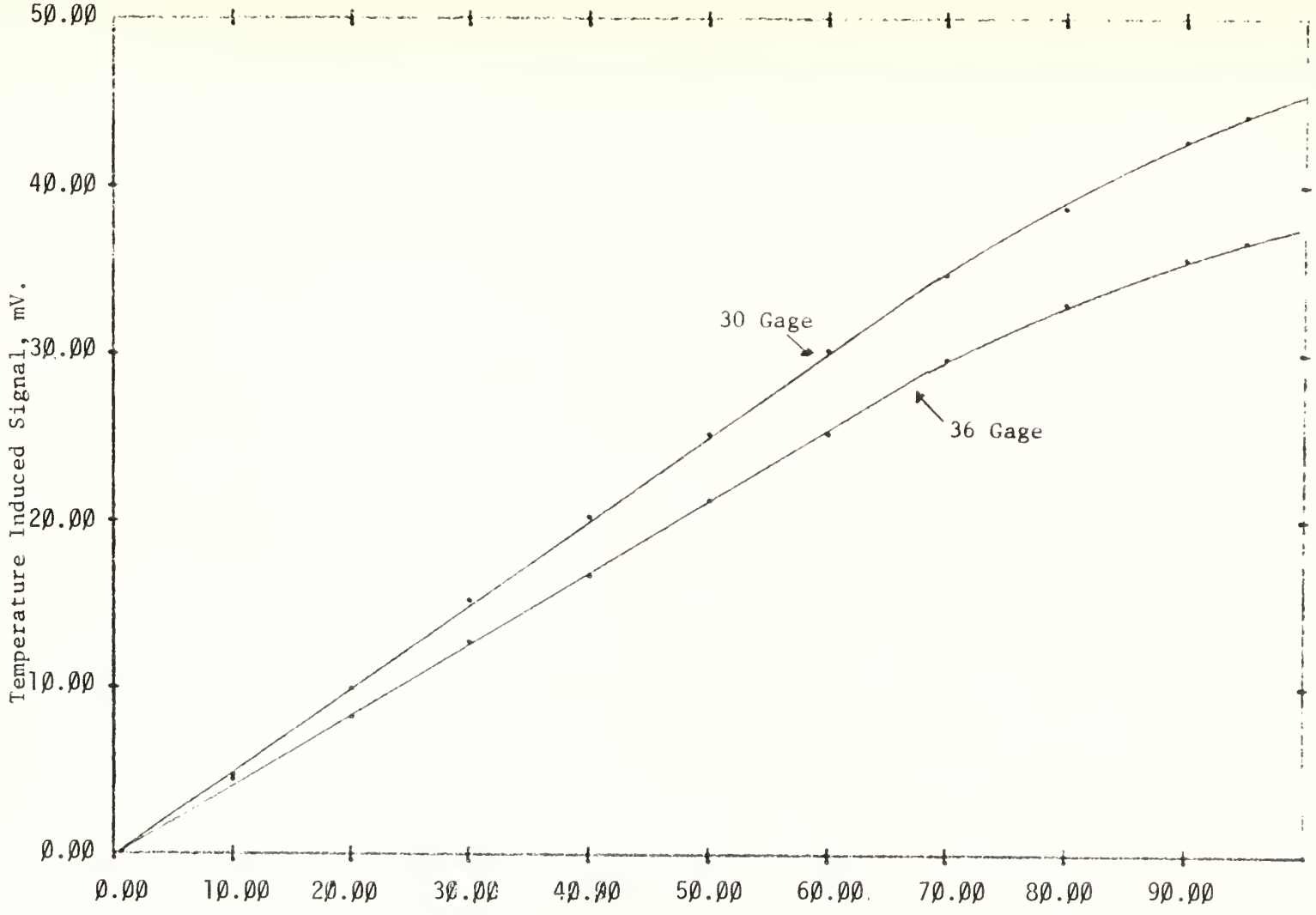


Figure 4. Thermocouple Calibration Curves

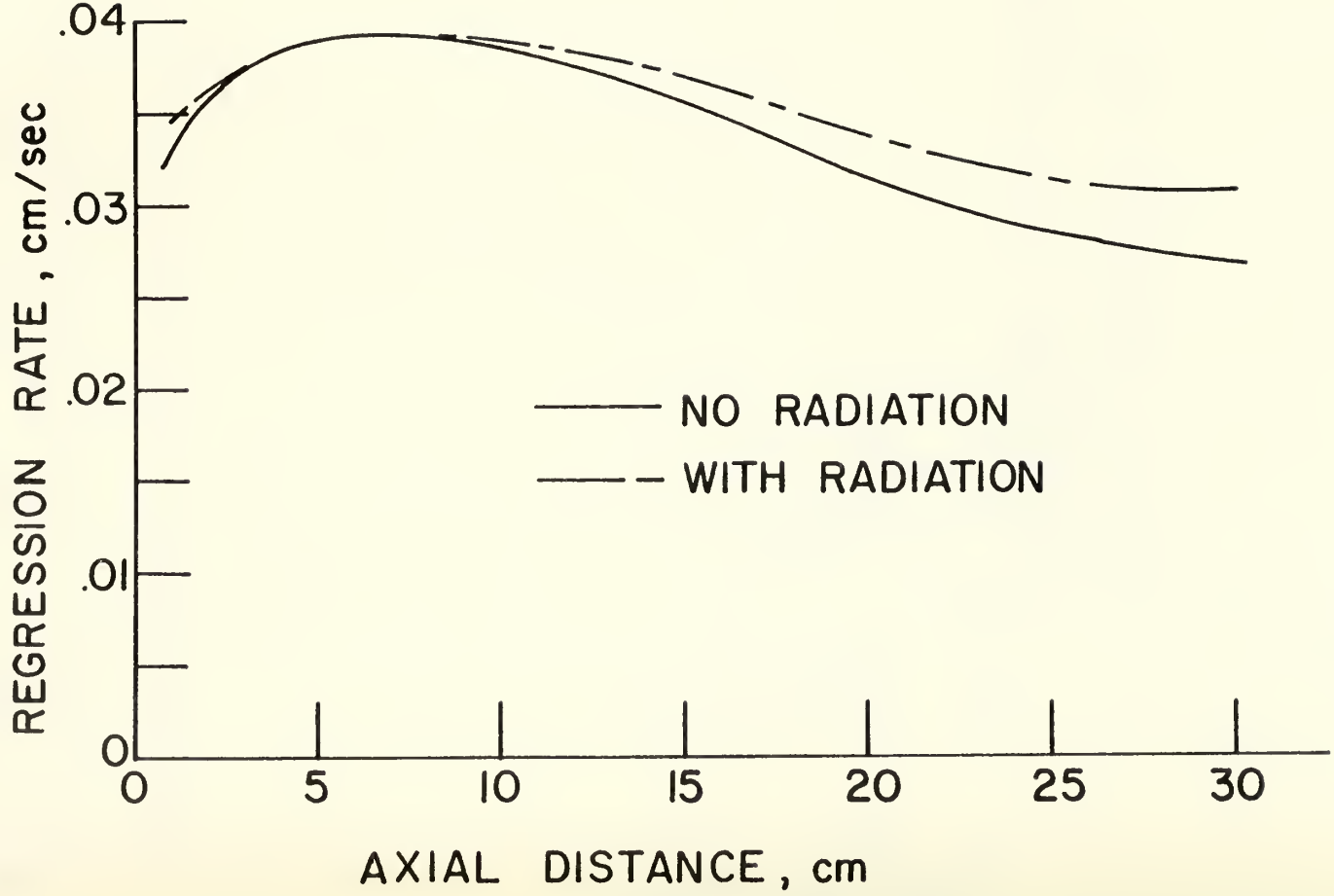


Figure 5. Effect of Radiation on the Predicted Fuel Regression Rates

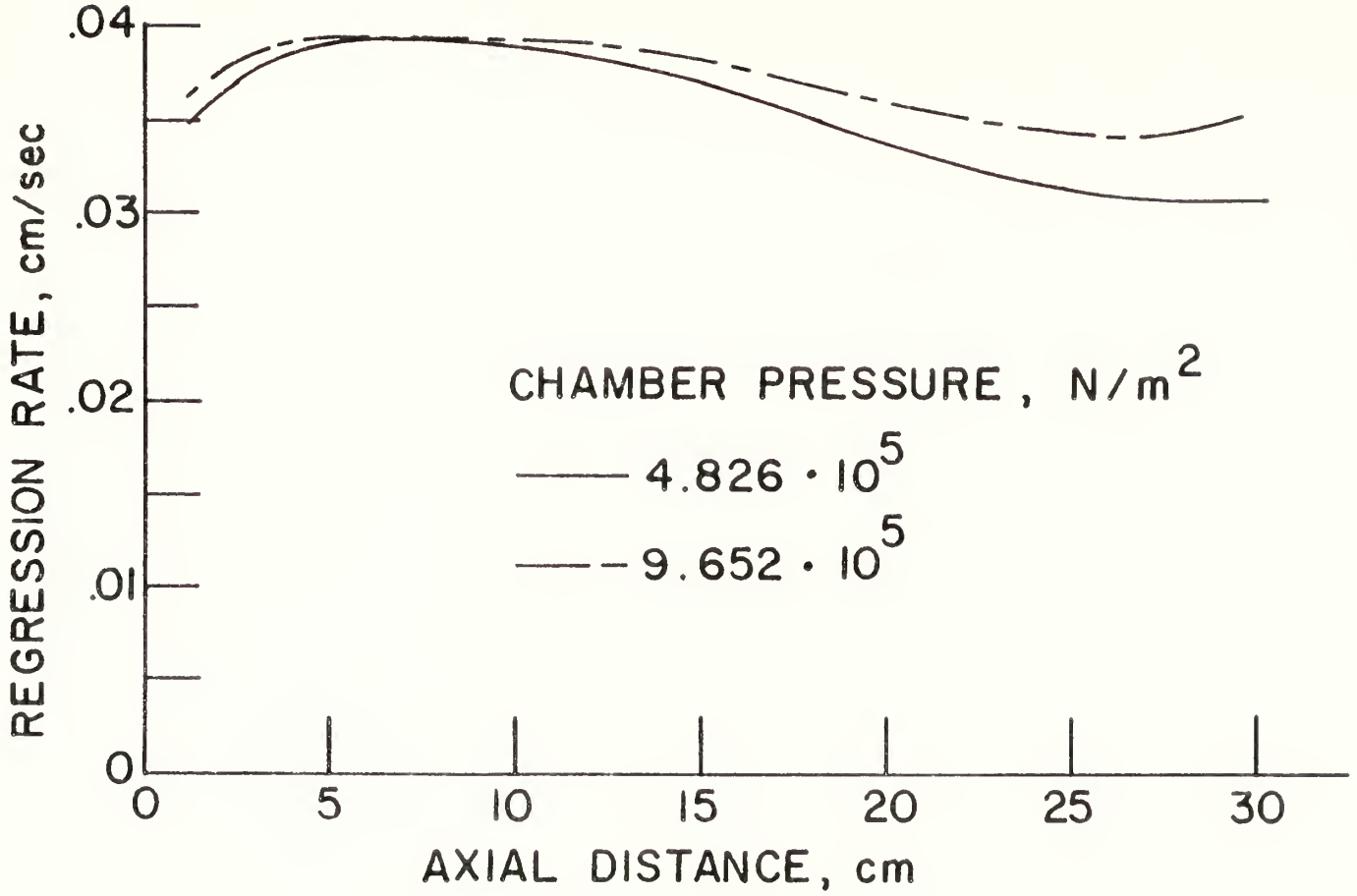


Figure 6. Effect of Pressure on the Predicted Fuel Regression Rates

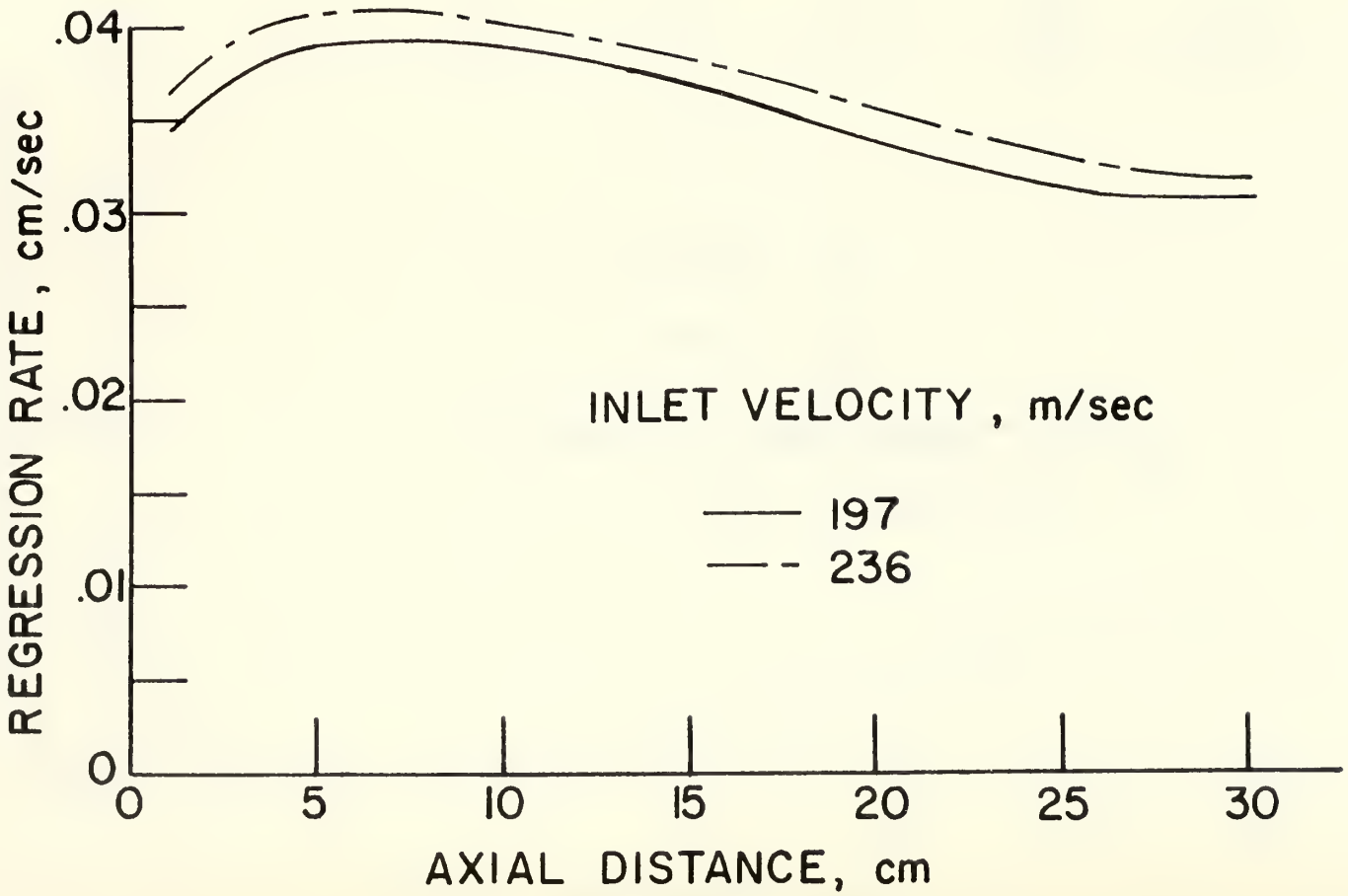


Figure 7. Effect of Inlet Velocity on the Predicted Fuel Regression Rates

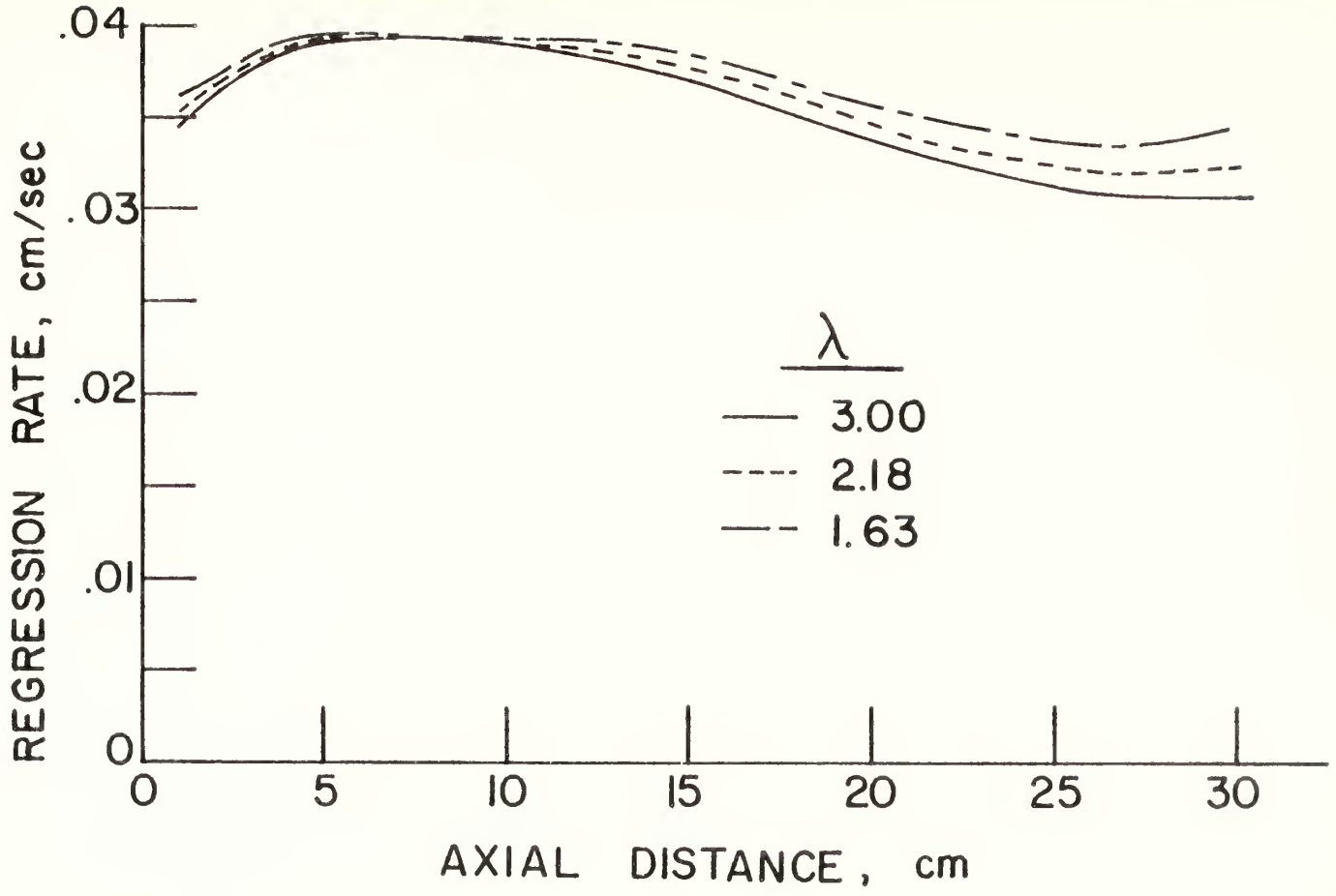


Figure 8. Effect of Increasing Radiation on the Predicted Fuel Regression Rates

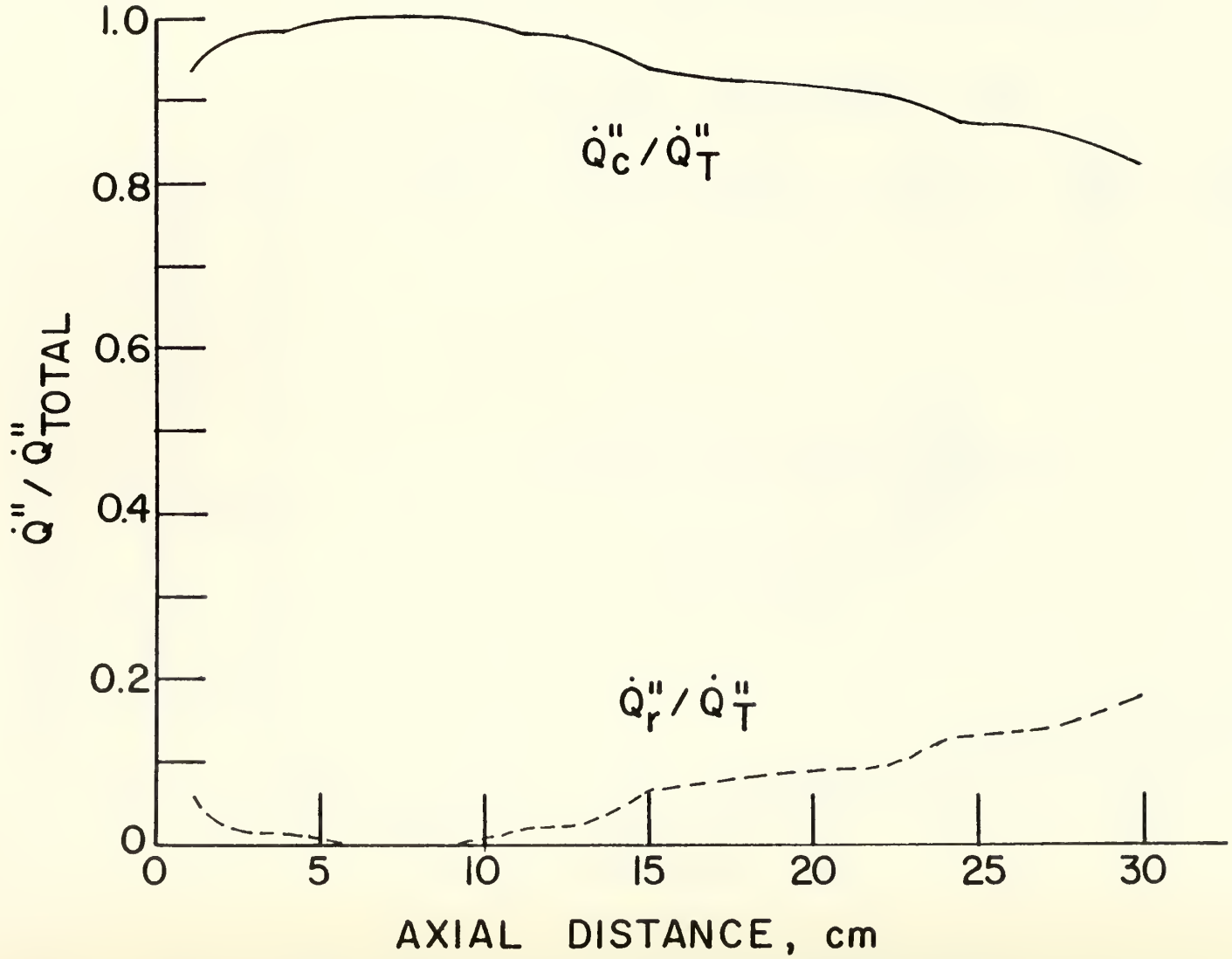


Figure 9. Predicted Distribution of Radiation Along the Fuel Grain

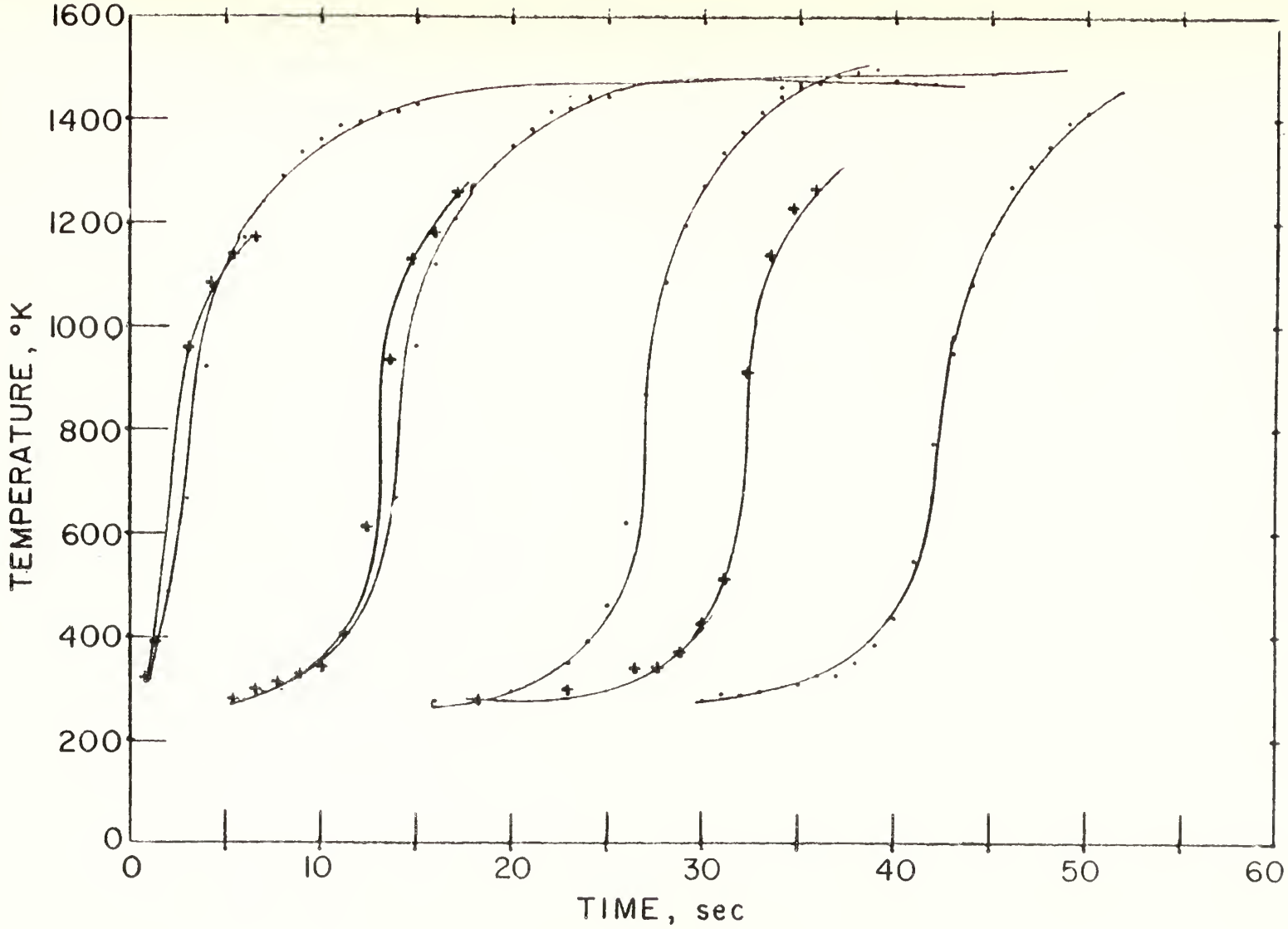


Figure 10. Temperature vs. Time (No Bypass Air)

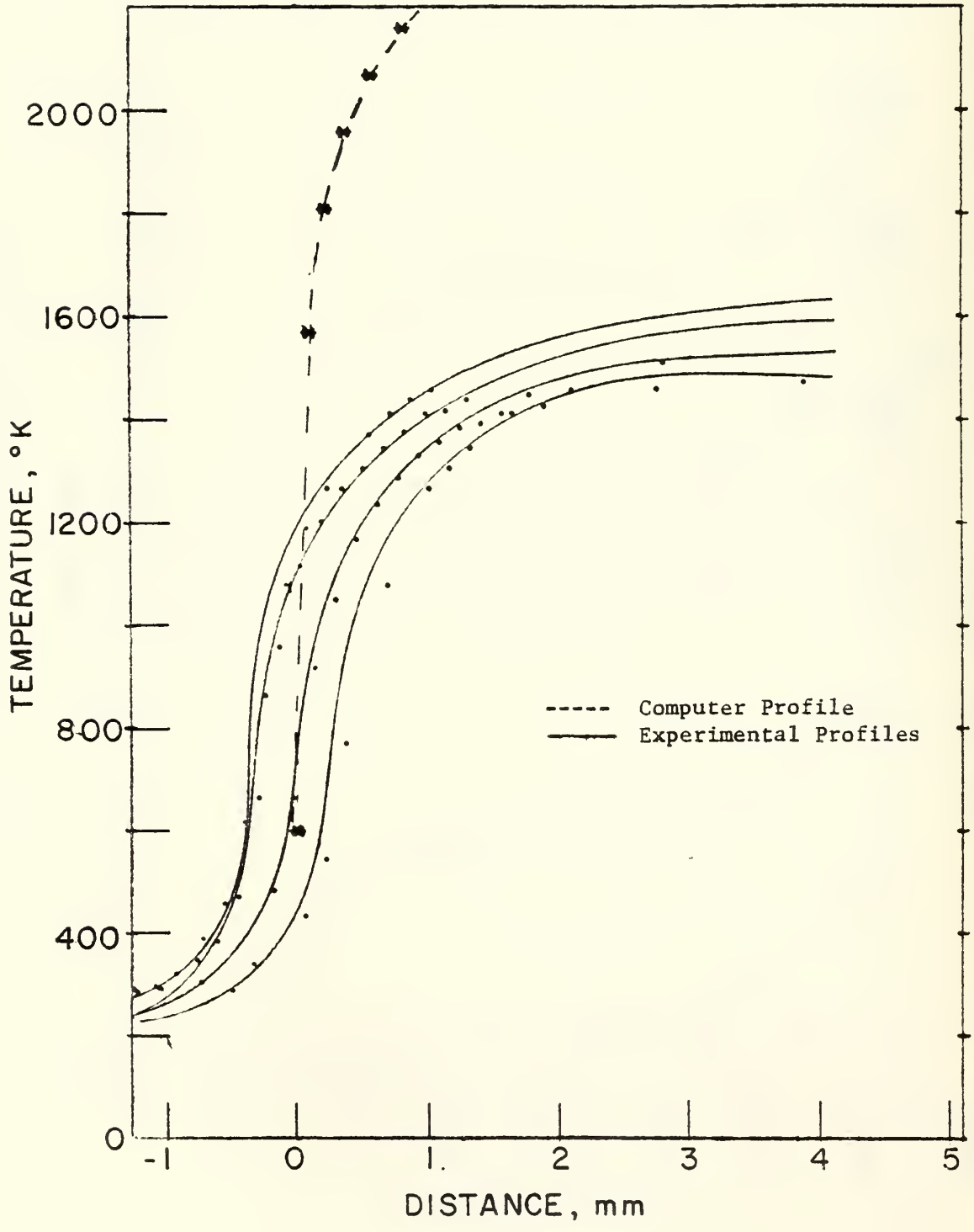


Figure 11. Radial Temperature Profiles (No Bypass Air)

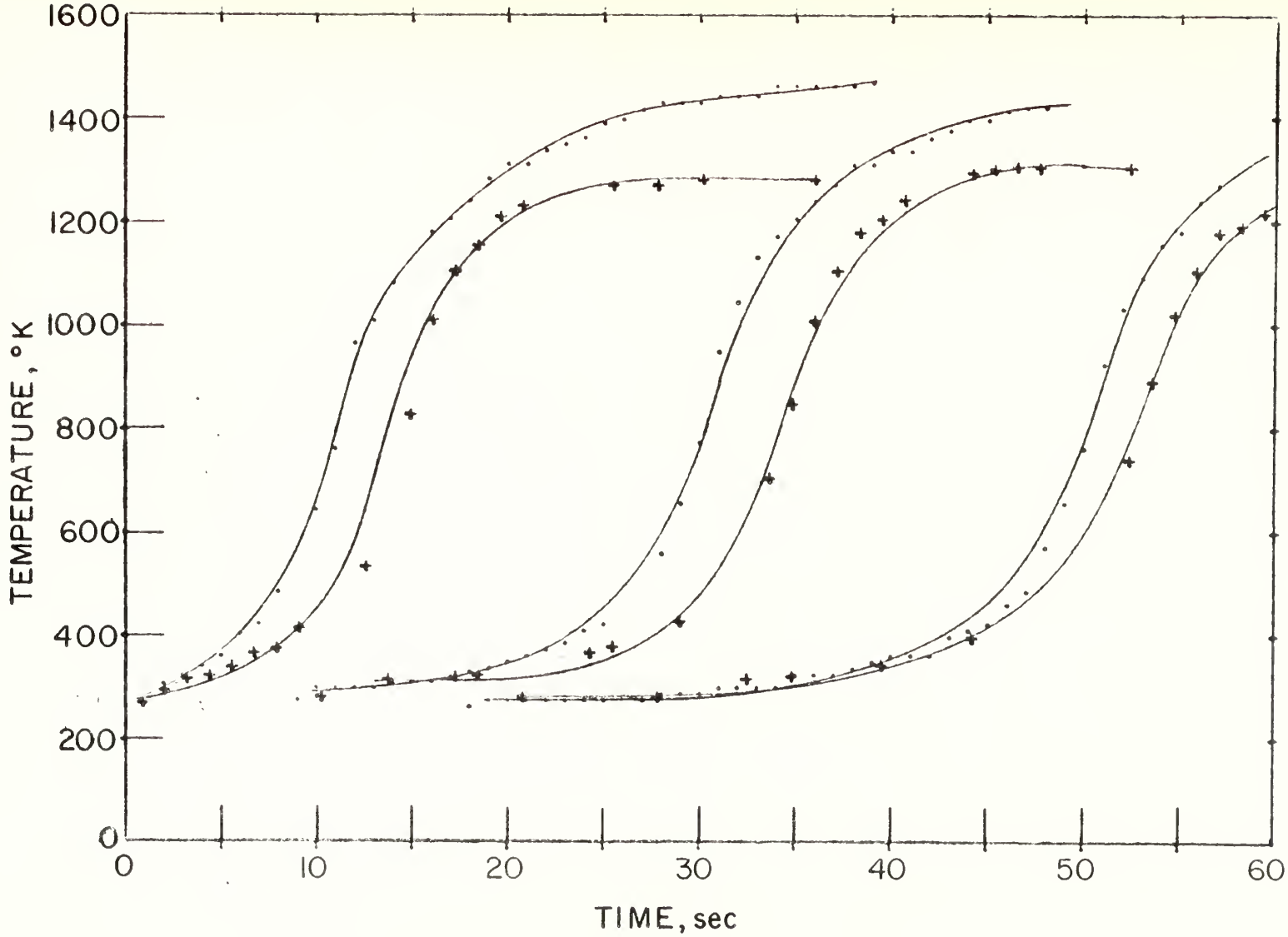


Figure 12. Temperature vs. Time (Bypass)

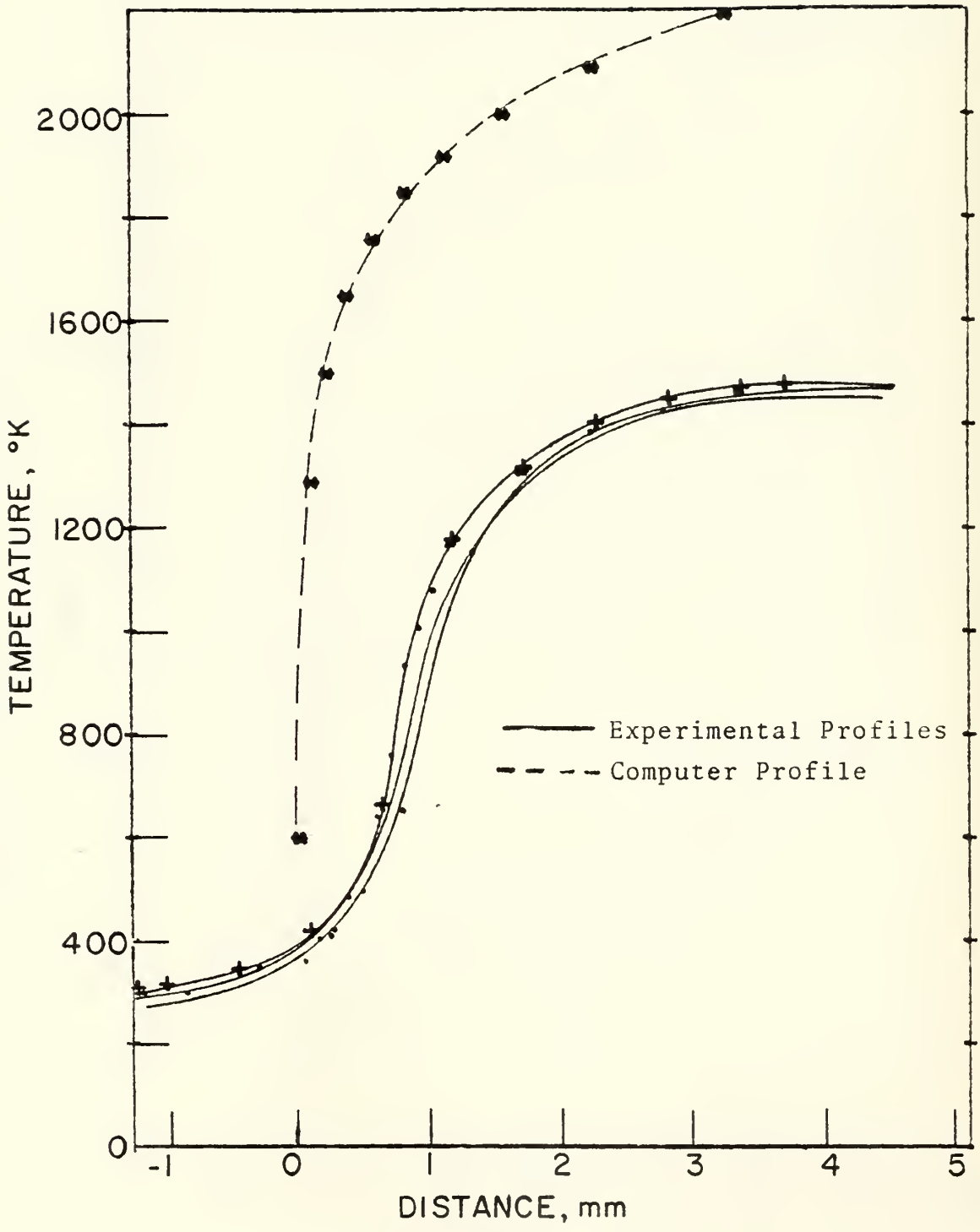


Figure 13. Radial Temperature Profiles ((Bypass)

## VI. REFERENCES


1. Netzer, D. W., Modeling Solid-Fuel Ramjet Combustion, Journal of Spacecraft and Rockets, Volume 14, Number 12, p. 762-766, December 1977.

2. Boaz, L. D., and Netzer, D. W., An Investigation of the Internal Ballistics of Solid Fuel Ramjets, NPS Report NPT-57Nt73031A, March 1973.

3. Phaneuf, Jr., J. T., and Netzer, D. W., Flow Characteristics in Solid Fuel Ramjets, NPS Report NPS-57Nt74081, May 1974.

4. Mady, C. J., Hickey, P. J., and Netzer, D. W., An Investigation of the Combustion Behavior of Solid Fuel Ramjets, NPS Report NPS-57Nt77092, September 1977.

5. Mady, C. J., Hickey, P. J., and Netzer, D. W., Combustion Behavior of Solid Fuel Ramjets, JSR, Vol. 15, No. 3, pp. 131-132, May-June 1978.

6. Hewett, M. E., and Netzer, D. W., Application of Light Extinction Measurements to the Study of Combustion in Solid Fuel Ramjets, NPS Report NPS-67-78008, November 1978.

7. Stevenson, C. A., and Netzer, D. W., A Primitive Variable Computer Model for Combustion Within Solid Fuel Ramjets, NPS Report NPS67-79-010, October 1979.

8. Pun, W. M., and Spalding, D. B., A General Computer Program for Two-Dimensional Elliptic Flows, Imperial College of Science and Technology, Report No. HTS/76/2, August 1977.

9. Jones, W. P., and Launder, B. E., The Predictions of Laminarization with a Two-Equation Model of Turbulence, INT. J. Heat Mass, Transfer, Vol. 15, pp. 68-87, 1972.

10. Launder, B. E., and Spalding, D. B., Lectures in Mathematical Models of Turbulence, 2nd ed., Academic Press, 1976.

11. Kays, W. M., Convective Heat and Mass Transfer, McGraw-Hill, 1966.

12. Marxman, G. A., Boundary Layer Combustion in Propulsion, Eleventh Symposium (International) on Combustion, The Combustion Institute, p. 263, Pittsburg, 1967.

13. Marxman, G. A., Woolridge, C. E., and Muzzy, R. J., Fundamentals of Hybrid Boundary-Layer Combustion, Heterogeneous Combustion, Progress in Astronautics and Aeronautics, Vol. 15, p. 485, Academic Press, New York, 1964.

INITIAL DISTRIBUTION LIST

| | | No. of Copies |
|---|---|---|
| 1. | Defense Technical Information Center<br>Cameron Station<br>Alexandria, VA 22314 | 2 |
| 2. | Library<br>Code 0142<br>Naval Postgraduate School<br>Monterey, CA 93940 | 2 |
| 3. | Department Chairman, Code 67<br>Department of Aeronautics<br>Naval Postgraduate School<br>Monterey, CA 93940 | 1 |
| 4. | Professor D. W. Netzer<br>Department of Aeronautics<br>Naval Postgraduate School<br>Monterey, CA 93940 | 15 |
| 5. | Naval Air Systems Command<br>AIR-330<br>Washingtonton DC 20361 | 2 |
| 6. | Commanding Officer<br>Naval Weapons Center<br>China Lake, CA 9355 | |
| | Technical Library, Code 753 | 3 |
| | F. Zarlingo, Code 3246 | 3 |
| | K. Schadow, Code 388 | 1 |
| | W. Burdette | 1 |
| 7. | Chemical Systems Division<br>United Technologies<br>P. O. Box 358<br>Sunnyvale, CA 94088 | |
| | Technical Library | 1 |
| | R. Dunlap | 1 |
| | A. Holzman | 1 |
| | G. Jensen | 1 |
| | P. Willoughby | 1 |
| | P. LaForce | 1 |
| 8. | Chemical Propulsion Information Agency<br>APL-JHU<br>Johns Hopkins Road<br>Laurel, MD 20810 | 2 |
| 8. | AFARL<br>Wright-Patterson AFB, OH 45433 | |
| | R. D. Stull | 2 |